Monthly Notices
of the
ROYAL ASTRONOMICAL SOCIETY

Mon. Not. R. Astron. Soc. **406,** 1146–1151 (2010) doi:10.1111/j.1365-2966.2010.16744.x

An ingress and a complete transit of HD 80606 b

M. G. Hidas,[1,2,3★] Y. Tsapras[1,4★], D. Mislis,[5] A. N. Ramaprakash,[6] S. C. C. Barros,[7] R. A. Street,[1,2] J. H. M. M. Schmitt,[5] I. Steele,[8] D. Pollacco,[7] A. Ayiomamitis,[9] J. Antoniadis,[10] A. Nitsos,[10] J. H. Seiradakis,[10] S. Urakawa[11]

[1]*Las Cumbres Observatory Global Telescope, Goleta, CA 93117, USA*
[2]*Department of Physics, University of California, Santa Barbara, CA 93106, USA*
[3]*Sydney Institute for Astronomy, School of Physics, The University of Sydney, NSW 2006, Australia*
[4]*School of Mathematical Sciences, Queen Mary, University of London, Mile End Road, London E1 4NS*
[5]*Hamburger Sternwarte, Gojendergsweg 112, D-21029 Hamburg, Germany*
[6]*Inter-University Centre for Astronomy and Astrophysics, Ganeshkhind, Pune 411007, India*
[7]*Astrophysics Research Centre, School of Mathematics and Physics, Queen's University Belfast, Belfast BT7 1NN*
[8]*Astrophysics Research Institute, Liverpool John Moores University, Liverpool CH41 1LD*
[9]*Hellenic Astronomical Union, Athens, Greece*
[10]*Department of Physics, Section of Astrophysics, Astronomy and Mechanics, University of Thessaloniki, GR-54124 Thessaloniki, Greece*
[11]*Bisei Spaceguard Center, Japan Spaceguard Association, 1716-3 Ohrura, Bisei-cho, Ibara, Okayama 714-1411, Japan*

Accepted 2010 March 25. Received 2010 March 18; in original form 2010 February 4

ABSTRACT

We have used four telescopes at different longitudes to obtain near-continuous light-curve coverage of the star HD 80606 as it was transited by its ∼4-$M_{\rm Jup}$ planet. The observations were performed during the predicted transit windows around 2008 October 25 and 2009 February 14. Our data set is unique in that it simultaneously constrains the duration of the transit and the planet's period. Our Markov Chain Monte Carlo analysis of the light curves, combined with constraints from radial-velocity data, yields system parameters consistent with previously reported values. We find a planet-to-star radius ratio marginally smaller than previously reported, corresponding to a planet radius of $R_{\rm p} = 0.921 \pm 0.036 R_{\rm Jup}$.

Key words: stars: individual: HD 80606 – planetary systems.

1 INTRODUCTION

An important class of the ∼400 extra-solar planets known to date is the so-called hot Jupiters, orbiting a fraction of an astronomical unit from their host star. Many of these have significantly larger radii than planets of similar mass in our Solar system. This has been a challenge for theoretical models of their structure. The intense radiation and tidal forces from the host star are expected to play a significant role (e.g. Bodenheimer, Lin & Mardling 2001; Burrows et al. 2007). For planets in highly eccentric orbits, both of these factors vary greatly over the course of the orbit. Thus, such planets provide interesting tests for models of the structure and dynamics of planetary atmospheres (e.g. Irwin et al. 2008, and references therein).

A planet in a 111-d orbit around the star HD 80606 was first detected in radial-velocity observations (Naef et al. 2001). The minimum mass ($M_{\rm p} \sin i$) of the planet is 3.9 times the mass of Jupiter. HD 80606 b has the most eccentric orbit of all the extra-solar planets known to date ($e = 0.93$). Infrared (8 μm) observations clearly show the rapid heating of the planet's atmosphere during periastron passage (Laughlin et al. 2009, hereafter L09). Laughlin et al. also reported detection of a secondary eclipse, implying that the orbital inclination is close to 90° and motivating efforts to observe a transit of the planet in front of the star.

In early 2009, several groups observed a transit egress in photometry (Fossey, Waldmann & Kipping 2009; Garcia-Melendo & McCullough 2009; Moutou et al. 2009) and spectroscopy (Moutou et al. 2009). Analyses of these data, together with old and new radial-velocity measurements, provided the first constraints on the planet's radius and actual mass, as well as its orbital parameters (Pont et al. 2009, hereafter P09; Gillon 2009, hereafter G09). These analyses are limited by the fact that the duration of the transit is not constrained, which in turn increases uncertainties in the system parameters. Winn et al. (2009, hereafter W09) report multiple observations of the transit ingress in 2009 June and combine their data with the earlier ingress observations and Keck radial-velocity data to constrain the transit duration.

In this paper, we present previously unpublished multisite photometric observations of a complete transit of HD 80606 b on 2009 February 14 and an ingress on 2008 October 25. We describe the observations and the resulting data sets in Section 2. In Section 3 we describe the methods we used to analyse our data, and in Section 4 we report and discuss the results.

★E-mail: mhidas@lcogt.net (MGH); ytsapras@lcogt.net (YT)

2 OBSERVATIONS

We observed HD 80606 with four telescopes during predicted transit windows around 2008 October 25 (hereafter Oct08) and 2009 February 14 (hereafter Feb09).[1] As no transit or secondary eclipse had been reported at the time, these windows were ∼24 h long.

Where available, we observed through Bessell *B* and *R* filters, alternating between them every few minutes. The one exception to this is noted below. In all cases we deliberately defocused the telescope [often to the point where the point spread function (PSF) became an annulus, but taking care that the target and its binary companion do not blend]. This allowed longer exposure times without saturating the detector. More importantly, it meant that each star was measured by a large number of pixels, reducing the effects of flat-fielding errors and pointing drift on the photometry.

Besides those mentioned below, we also attempted observations at Bisei Astronomical Observatory in Japan, Kryonerion Astronomical Station in Greece and an amateur observatory in Athens, Greece, but did not yield any useful data due to adverse weather.

2.1 Faulkes Telescope North, Hawaii

The 2-m Faulkes Telescope North (FTN) – part of the Las Cumbres Observatory Global Telescope Network (LCOGT.net) – is located at Haleakala in Hawaii. We used FTN and a Merope camera with a 2k×2k e2v CCD (binned 2 × 2). Observations were conducted by the telescope's Robotic Control System, alternating between sets of 37-s exposures in *B* and 20-s exposures in *R*. We only obtained useful data for the Feb09 transit. Images were processed by our automated pipeline to remove the effects of bias, dark current and CCD sensitivity variations.

2.2 IUCAA Girawali Observatory, India

Observations were carried out from the Inter-University Centre for Astronomy and Astrophysics (IUCAA) Girawali Observatory (IGO; Das et al. 1999), and we obtained useful data during the Feb09 transit window.

We used the IUCAA Faint Object Spectrograph Camera (IFOSC; Gupta 2002) mounted on the direct Cassegrain focus of the IGO 2-m telescope. Exposure times were 15–30 s in *B* and 4–10 s in *R*. Images were corrected using overscan strips and master bias frames followed by flat-fielding, using the IFOSC photometry pipeline package developed under IRAF.

2.3 Oskar-Lühning Telescope, Germany

We observed HD 80606 on three nights in Feb09 with the 1.2-m Oskar-Lühning Telescope (OLT) at Hamburg Observatory. We changed filters after every five exposures, with exposure times of 55 s in *B* and 35 s in *R*. Images were bias-/dark-subtracted and flat-fielded using the *FIGARO* subroutine in the Starlink software package.

2.4 Liverpool Telescope, Canary Islands

Liverpool Telescope (LT; Steele et al. 2004) data were obtained on 2008 October 25 and 26 using the RISE frame transfer wide field camera (Steele et al. 2008) in a 2 × 2 binned mode, giving a pixel scale of 1.07 arcsec pixel^{-1}. The filter employed consisted of 2-mm Schott KG5 bonded to 3-mm Schott OG515, giving half–maximum transmission from 515 to 695 nm (i.e. roughly equivalent to a combined $V + R$ filter). An exposure time of 1 s was used, with effectively no dead time between exposures. All data were dark-subtracted and flat-fielded using the ULTRACAM pipeline, which is optimized for time series photometry. A master twilight flat was constructed from a median of several hundred frames.

2.5 Photometry

Starting with the calibrated images, we performed aperture photometry on all data sets in the same manner, with the exception of the LT data.

For each instrument, a single master image was selected and used as a reference for all images obtained with that instrument. The coordinates of the target and reference stars in the master image were obtained by convolving it with a copy of the PSF from the same image and then running DAOFIND in IRAF on the result.

All other images were registered to the master using direct correlation with the XREGISTER task. The master list of coordinates was then transformed into the reference frame of each image. DAOPHOT was used to obtain photometry in a range of apertures (slightly different for each instrument). The photometric scatter was smallest in the largest aperture used for all data sets (radius of 11 arcsec for FTN, 8 arcsec for IGO and 10 arcsec for OLT).

For the LT data, we also performed aperture photometry, trying out different aperture radii, choosing the one that minimized the noise (8.6 arcsec). Apertures were centred in each frame by cross-correlation of the image with a Gaussian.

We measured the flux of HD 80606 relative to its binary companion HD 80607, as it was the only reference star available in all data sets. Additional stars in the fields of view of some of the instruments were significantly fainter and of different colours and were only used as check stars.

We prepared each light curve for fitting by taking the following steps.

(i) We removed points more than 5σ from the median of the time series.

(ii) We normalized the flux values to a median of 1 for points well outside the transit.

(iii) We binned the light curve into 10-min bins in order to reduce the number of points to fit. We estimated uncertainties as the standard deviation of the values within each bin, divided by the square root of the number of points in the bin.[2]

3 ANALYSIS

The complete set of useful data we obtained is shown in Fig. 1. It includes a transit ingress observed by the LT in 2008 October and – between the FTN, IGO and OLT data sets – nearly continuous coverage of the transit in 2009 February in two filters.

3.1 Light-curve model

We modelled the HD 80606 system as a planet of radius R_p, orbiting a star of radius R_*, with orbital period P, semimajor axis a, eccentricity e and inclination i (relative to our line of sight). The argument of periastron is ω and the planet passes there at time T_p.

[1] We obtained the predicted transit windows from http://transitsearch.org.

[2] For bins containing only a single original point, we estimated the uncertainty based on the nearest two bins with at least two points.

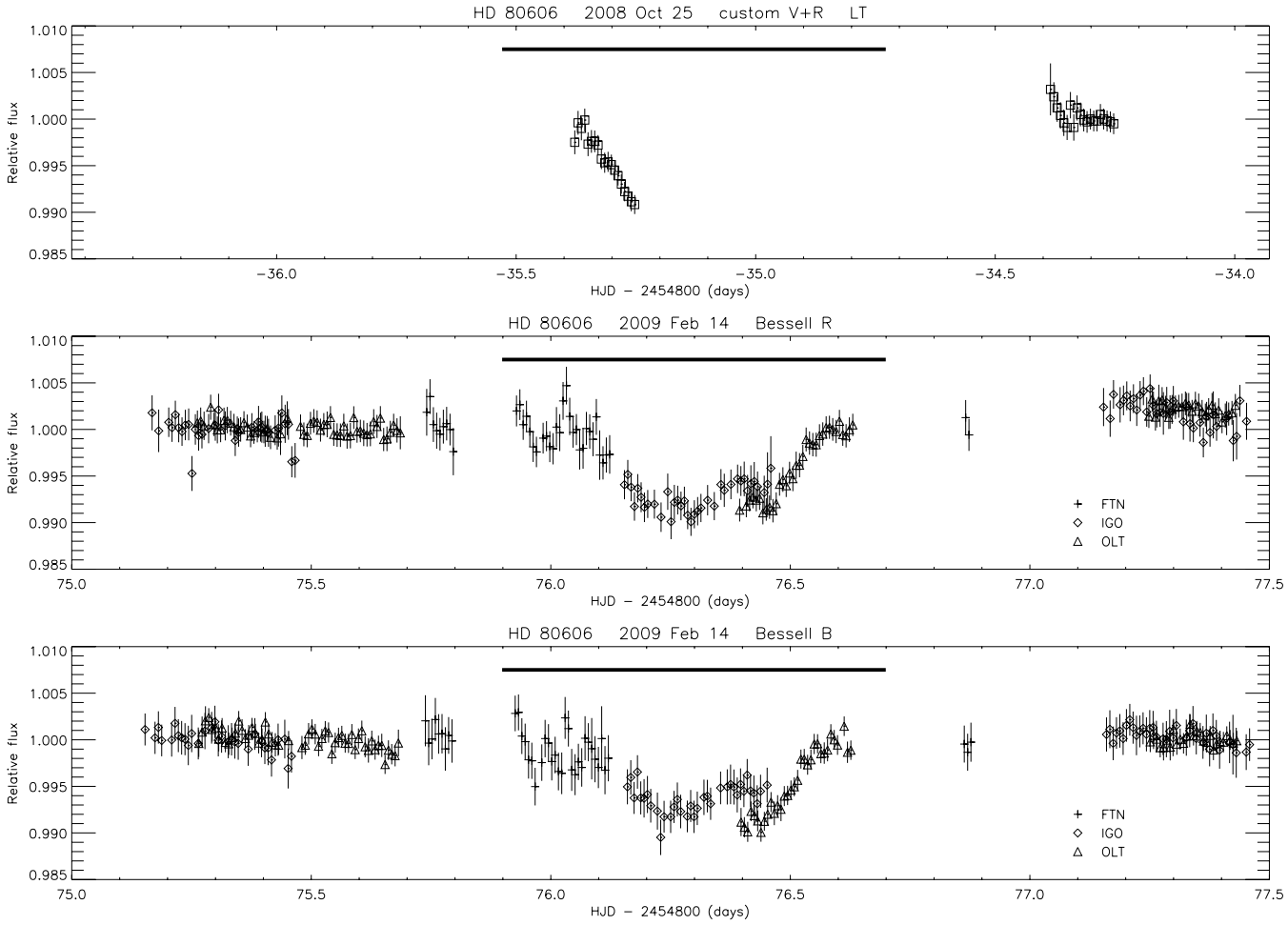

Figure 1. The complete data set analysed in this paper: a transit ingress of HD 80706 b observed with the LT (top panel) and the following transit observed by the FTN, the IGO's 2-m telescope and the OLT. The middle and bottom panels show the same transit in the Bessell *R* and *B* bands, respectively. The horizontal bar across the top shows the section of data used in the fit. The error bars indicate the weights used in the fit, i.e. they include the statistical uncertainty as well as the red noise estimate (σ_i and $\sigma_{r,s}$ in equation 1).

To obtain light curves for a given set of system parameters, we first solved Kepler's equation using the Newton–Raphson iteration and then calculated the planet's position in its orbit and its distance (in the plane of the sky) from the centre of the star. Taking this as input, the analytical transit models of Mandel & Agol (2002) provided the relative fluxes expected for our physical model. We assumed a quadratic limb-darkening law, with coefficients interpolated from the tables of Claret (2000).[3]

3.2 Fitting

We determined the parameters of the model using a Markov Chain Monte Carlo (MCMC) approach similar to that of Torres, Winn & Holman (2008) and references therein. Briefly, from a random starting point, small jumps in parameter space are generated, and each new point is evaluated using a merit function (χ^2). If the jump results in a lower χ^2, it is executed (i.e. the new point becomes the next 'link' in the chain). Otherwise, it is only executed with a probability $\exp(-\Delta\chi^2/2)$. If a jump is not executed, the previous point is repeated in the chain. After a large number of jumps, the result is a distribution of points in parameter space that approximates the joint posterior probability density of all the parameters given in our data.

We used a merit function of the form

$$\chi^2 = \sum_{i=1}^{N} \frac{(n_s f_i - m_i)^2}{\sigma_i^2 + \sigma_{r,s}^2} + \sum_{j=1}^{M} \frac{(v_j - c_j)^2}{\sigma_{c,j}^2}. \quad (1)$$

The first sum is the usual χ^2 statistic and is related to the probability of the data given in the model. For each of N data points, f_i is the measured relative flux, m_i is the model at that point, σ_i is the statistical uncertainty in the measurement and $\sigma_{r,s}$ is an estimate of the correlated noise in each data set (see below). We also included a normalization factor n_s (constant within each data set s) to allow the model to match the out-of-transit relative flux.

The additional terms in the merit function represent constraints from previously published measurements, as detailed in Table 1. In each case, a value calculated from our model (v_j) is being compared to a measured value (c_j) with corresponding uncertainty ($\sigma_{c,j}$). We included the time and duration of the secondary eclipse from L09 as

[3] Based on the stellar parameters reported by Naef et al. (2001), we obtained the limb-darkening coefficients $u_1 = 0.5043$, $u_2 = 0.2535$ in the *R* band and $u_1 = 0.8827$, $u_2 = -0.0166$ in the *B* band. For the LT data set ($V + R$), we used the mean of the coefficients for *V* and *R*: $u_1 = 0.6117$, $u_2 = 0.1853$.

Table 1. Measurements by L09 included as constraints in the MCMC merit function. The three columns correspond to v_j, c_j and $\sigma_{c,j}$, respectively, in equation (1). The last two rows refer to the epoch and duration (2nd to 3rd contact) of the secondary eclipse.

Parameter	Value	Uncertainty
Orbital period, P (d)	111.4277	0.0032
Orbital eccentricity, e	0.9327	0.0023
Argument of periastron, ω (deg)	300.5	0.2[a]
Epoch of mid-eclipse (HJD)	245 4424.736	0.003
Total-eclipse duration (d)	0.070	0.009

[a]This is our conservative estimate of the uncertainty (see Section 3.2). The value reported by L09 is $\omega = 300\overset{\circ}{.}477 \pm 0\overset{\circ}{.}0045$.

well as the period, eccentricity and argument of periastron they derived from Keck radial-velocity data. W09 note that the uncertainty in ω quoted by L09 is likely to be underestimated. Indeed, both W09 and P09 analyse larger data sets and find uncertainties of $\sim 0\overset{\circ}{.}2$ in ω. Therefore, we adopt the value of ω from L09, but only give it a weight corresponding to $\sigma_{c,\omega} = 0.2$. We did not include constraints from any other photometric observations in order to obtain results as independent as possible from other analyses.

During the MCMC simulation, we varied the following parameters: $a/R_*, P, T_\mathrm{p}, e'$ (see below), $\omega, b = a/R_* \cos i$ (proportional to the transit impact parameter), R_p/R_* and a normalization factor for each instrument/filter combination (n_s). A total of 14 parameters were varied. In order to avoid strong correlations which restrict the movement of the MCMC chain through parameter space, we used combinations of some of the physical parameters that are more directly constrained by the data (e.g. the radius ratio instead of the absolute radii). When eccentricity was included as one of the varied parameters, correlations caused different MCMC chains to converge to different locations in (P, e, ω) space. We found that most of the variation in e over all chains could be described as a linear function of P and ω. Thus, we replaced e with $e' = e - k_0 P - k_1 \omega$, where $k_0 = 0.035$ and $k_1 = -0.0035$ were determined from the previous fit. This resulted in the MCMC simulation moving more freely through parameter space and a more continuous distribution of points when the chains were combined.

We generated jumps by adding a Gaussian-distributed random value to one of the varied parameters (randomly chosen) at each iteration. We tuned the jump sizes for each parameter so that approximately 25–50 per cent of jumps were executed.

3.3 Correlated noise

Each of our data sets contains some noise that is correlated in time due to gradual variations in atmospheric or instrumental factors. The *internal* uncertainties we estimated for each data point (as described in Section 2.5) do not measure this *red noise*, yet it can significantly affect the results of our analysis (Pont, Zucker & Queloz 2006). To account for the effect of red noise, we reduced the weight of each point in the merit function (equation 1) with an additional noise term, $\sigma_{r,s}$, which we estimated as follows. We first performed an initial fit setting $\sigma_{r,s}$ to an optimistic 0.0005 for all data sets. For each data set s (of N_s points), we then found the value of $\sigma_{r,s}$ for which the reduced χ^2

$$\chi_r^2 = \frac{1}{N_s - 8} \sum_{i=1}^{N_s} \frac{(f_i - m_i)^2}{\sigma_i^2 + \sigma_{r,s}^2} \qquad (2)$$

was equal to unity.[4] We then repeated the fit and checked that the values of $\sigma_{r,s}$ were self-consistent. The final values used were LT: 0.001, FTN(R): 0.0016, IGO(R): 0.0015, OLT(R): 0.0012, FTN(B): 0.0019, IGO(B): 0.0017, OLT(B): 0.001. The average internal uncertainty of data used in the fit was only 0.0006, so – as is generally the case in such analyses – red noise is the main factor limiting the accuracy of our results.

4 RESULTS AND DISCUSSION

For our final fit, we created 25 independent chains of 42 000 steps each and discarded the first 2000 steps of each chain to minimize the effect of the (randomly chosen) starting points on our results. Combining the remaining steps of all the chains, the resulting distribution of parameter values approximates their joint probability density. For each parameter, we report the median of this distribution as the 'best-fitting' value[5] and the boundaries of the central 68 per cent as the 1σ uncertainties.

The results thus obtained are shown in Table 2 and the fit itself is compared to the data in Fig. 2. The reduced χ^2 for this fit is 0.63, which suggests that we have slightly overestimated the uncertainties in our data. Thus, the uncertainties in our results are somewhat conservative. We also note that there are unavoidable correlations between some parameters. Besides the P–e–ω correlation mentioned in Section 3.2, the strongest of these is between $a/R_*, b$ and R_p/R_*. There are also significant correlations between T_p and ω and also between R_p/R_* and the normalization factor for the IGO data. The uncertainties in results include the effects of all these correlations.

Since we used the values of the period (P), eccentricity (e) and argument of periastron (ω) from L09 as direct constraints in the fit, we obtained results that agree with those values. We did find a larger uncertainty for ω, but a more precise value for the eccentricity.

Our results also agree well with the parameters reported by P09, G09 and W09. The only significant exception to this is the period, where our result is 3σ smaller than the other analyses. We note, however, that we have essentially forced our simulations to agree with the period reported by L09. If we repeat our fit without the direct constraints on P, e and ω (see Section 3.2), the best-fitting period is almost unchanged, but the uncertainty in its value is four times greater. This means that our photometric data are in fact consistent with the period reported by P09, G09 and W09.

We also find a planet-to-star radius ratio that is marginally smaller (by 1.8σ) than the values reported by W09 and G09. A possible cause for this is the nature of our data from the IGO, which contains the majority of the in-transit points, but no out-of-transit points on the same night. This means that the normalization of those data is not strongly constrained and leads to the correlation noted above. In addition, the IGO data appear to show a significant systematic trend in the middle of the transit, which we were unable to remove by de-correlation against any physical parameters of the observations (such as airmass or position on the CCD).

[4] The effective number of parameters for this χ^2 is 8, consisting of the seven physical parameters and one normalization factor n_s for the given data set.
[5] As P09 point out, the set of parameters thus obtained does not actually correspond to the MCMC step with the lowest χ^2 value. This is because each parameter's median value comes from a different step in the chain.

Table 2. Physical parameters of the HD 80606 b system obtained from the MCMC fit.

Parameter	Median	Uncertainty
Scaled semimajor axis, a/R_*	101.2	$-5.5, +6.9$
Orbital period, P (d)	111.4273	± 0.0031
Orbital eccentricity, e	0.933 69	$\pm 0.000\,68$
Epoch of periastron, T_p (HJD)	245 4424.8575	± 0.0040
Argument of periastron, ω (deg)	300.53	± 0.19
Orbital inclination, i (deg)	89.341	$-0.063, +0.073$
Planet/star radius ratio, R_p/R_*	0.0967	$-0.0035, +0.0032$
Planet radius, R_p [a] (R_{Jup})	0.921	± 0.036
Epoch of mid-transit (HJD)	245 4876.3173	± 0.0036
Complete transit duration ($t_4 - t_1$, h)	12.14	± 0.36
Ingress/egress duration ($t_2 - t_1$, h)	2.33	± 0.37

[a] Using $R_* = 0.978 \pm 0.015\,R_\odot$ (P09).

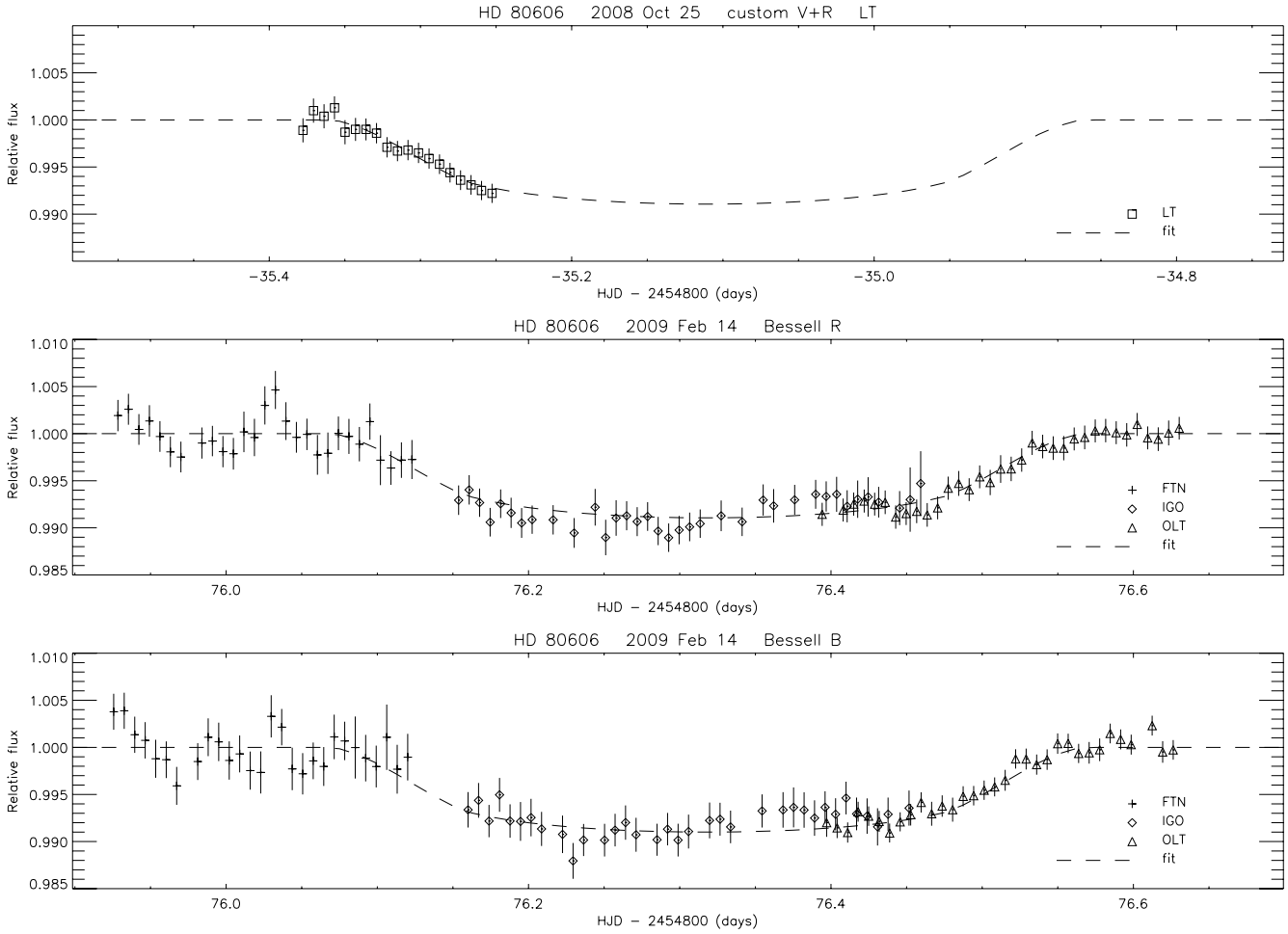

Figure 2. Close-up of the data used in the fit, along with the best-fitting model obtained from MCMC simulations. Symbols and error bars are the same as in Fig. 1; only the horizontal scale is different.

5 CONCLUSION

We have obtained multisite observations of a transit ingress and a complete transit of HD 80606 b across its host star. We analysed these data independently of any other photometric data and found system parameters consistent with previously reported values.

These observations were made using four telescopes at different sites. This allowed us to obtain near-continuous coverage of this 12-h event. However, the differences between the instruments, telescopes and time-allocation procedures were, to an extent, limitations on our ability to obtain a uniform data set. In the near future, the completion of LCOGT's network of 1-m robotic telescopes (Brown et al. 2010) will greatly facilitate observations of this kind, providing near-identical instrumentation at a number of sites, under the control of a flexible, central scheduling system.

ACKNOWLEDGMENTS

We are grateful to Greg Laughlin for pointing out the opportunity to observe this transit. We thank Tom Marsh for the use of the ULTRACAM pipeline.

REFERENCES

Bodenheimer P., Lin D. N. C., Mardling R. A., 2001, ApJ, 548, 466
Brown T. M. et al., 2010, BAAS, 41, 401
Burrows A., Hubeny I., Budaj J., Hubbard W. B., 2007, ApJ, 661, 502
Claret A., 2000, A&A, 363, 1081
Das H. K., Menon S. M., Paranjpye A., Tandon S. N., 1999, Bull. Astron. Soc. India, 27, 609
Fossey S. J., Waldmann I. P., Kipping D. M., 2009, MNRAS, 396, L16
Garcia-Melendo E., McCullough P. R., 2009, ApJ, 698, 558
Gillon M. 2009, MNRAS, submitted, preprint (arXiv:0906.4904) (G09)
Gupta et al., 2002, Bull. Astron. Soc. India, 30, 785
Irwin J. et al., 2008, ApJ, 681, 636
Laughlin G., Deming D., Langton J., Kasen D., Vogt S., Butler P., Rivera E., Meschiari S., 2009, Nat, 457, 562 (L09)
Mandel K., Agol E., 2002, ApJ, 580, L171
Moutou C. et al., 2009, A&A, 498, L5
Naef D. et al., 2001, A&A, 375, L27
Pont F., Zucker S., Queloz D., 2006, MNRAS, 373, 231
Pont F. et al., 2009, A&A, 502, 695 (P09)
Steele I. A. et al., 2004, in Oschmann J. M., ed, Proc. SPIE 5489, Ground-Based Telescopes. SPIE, Bellingham, p. 679
Steele I. A., Bates S. D., Gibson N., Keenan F., Meaburn J., Mottram C. J., Pollacco D., Todd I., 2008, in McLean I. S., Casali M. M., eds, Proc. SPIE 7014, Ground-Based and Airborne Instrumentation for Astronomy II. SPIE, Bellingham, p. 217
Torres G., Winn J. N., Holman M. J., 2008, ApJ, 677, 1324
Winn J. N. et al., 2009, ApJ, 703, 2091 (W09)

This paper has been typeset from a TEX/LATEX file prepared by the author.